ADVANCED MATERIALS
www.advmat.de

Quantum-Confined-Superfluidics-Enabled Moisture Actuation Based on Unilaterally Structured Graphene Oxide Papers

Yong-Lai Zhang, Yu-Qing Liu, Dong-Dong Han, Jia-Nan Ma, Dan Wang, Xian-Bin Li, and Hong-Bo Sun**

The strong interaction between graphene oxides (GO) and water molecules has trigged enormous research interest in developing GO-based separation films, sensors, and actuators. However, sophisticated control over the ultrafast water transmission among the GO sheets and the consequent deformation of the entire GO film is still challenging. Inspired from the natural "quantum-tunneling-fluidics-effect," here quantum-confined-superfluidics-enabled moisture actuation of GO paper by introducing periodic gratings unilaterally is reported. The folded GO nanosheets that act as quantum-confined-superfluidics channels can significantly promote water adsorption, enabling controllable and sensitive moisture actuation. Water-adsorption-induced expansion along and against the normal direction of a GO paper is investigated both theoretically and experimentally. Featuring state-of-the-art of ultrafast response (1.24 cm^{-1} s^{-1}), large deformation degree, and complex and predictable deformation, the smart GO papers are used for biomimetic mini-robots including a creeping centipede and a smart leaf that can catch a living ladybug. The reported method is simple and universal for 2D materials, revealing great potential for developing graphene-based smart robots.

In the living systems, ultrafast ion and molecules transmission within a confined channel usually occurs in a quantum way, which mediates natural signal transmission, mass transfer, and energy conversion processes.[1] For instance, membrane proteins perceive a variety of stimuli such as taste, vision, touch, temperature, and pH by transient receptor potential ion channels.[2] The electrophorus of electric eel use electrocytes to generate voltages (over 600 V) by actuating ion channels.[3–5] The mechanical stimulation on Mimosa give rise to the fast flow of water through aquaporins leading to the falling down of the petiole, avoiding the damage.[6–8] The "quantum tunneling fluidics effect," recently defined as "quantum confined superfluidics (QSF)" by Jiang and coworkers,[9] has also inspired the rapid development of artificial QSF systems, for instance, funnel-shaped nanochannels,[10] smart DNA hydrogels integrated nanochannels,[11] and azobenzene-derivatives-modified polymer nanochannels,[12] toward various bionic applications that involve ultrafast ion and mass transport.

Recently, 2D materials, e.g., graphene,[13,14] graphene oxides (GO),[15–17] and MoS_2,[18] have been considered extremely promising candidates for developing layered QSF system due to their tunable interlayer-spacing and nanoporous structures. For instance, GO that possesses plenty of hydrophilic oxygen groups on their plane shows strong interaction with water molecules, e.g., forming hydrogen bonds.[19–21] Since the interlayer spacing of GO is generally between 6–12 Å,[16,22,23] which further depends on the water contents, GO films can be considered as a natural QSF system for ultrafast water transmission. It has been reported that the diffusion of water molecules between adjacent GO sheets is ultrafast since the process features ultralow friction and large slip lengths.[24] Based on the QSF effect, Geim's group found that GO membrane allow ultrafast permeation of water, which is at least 10^{10} times faster than He.[15] Subsequently, the same group demonstrated the tunable sieving of ions using GO membrane by controlling their interlayer spacing via humidity change.[16] In addition to the application in molecular/ion separation, the QSF effect of GO can also provide new design principle for other graphene-based devices such as desalination membranes, sensors, actuators, energy generation, and storage devices.[25–29] Taking actuators as an example, GO films enable rapid adsorption and ultrafast transmission of water molecules, which provides a feasibility of fabricating moisture responsive actuators by coupling another moisture-inert material layer.[30–32] Under moisture actuation, the selective adsorption of water molecules would directly generate a strain mismatch at the bilayer interface, leading to predictable deformation. However, in most cases, this kind of

Prof. Y.-L. Zhang, Y.-Q. Liu, Dr. D.-D. Han, J.-N. Ma, Dr. D. Wang, Prof. X.-B. Li, Prof. H.-B. Sun
State Key Laboratory of Integrated Optoelectronics
College of Electronic Science and Engineering
Jilin University
2699 Qianjin Street, Changchun 130012, China
E-mail: handongdong@jlu.edu.cn; hbsun@tsinghua.edu.cn
Prof. H.-B. Sun
State Key Laboratory of Precision Measurement Technology and Instruments
Department of Precision Instrument
Tsinghua University
Haidian district, Beijing 100084, China
The ORCID identification number(s) for the author(s) of this article can be found under https://doi.org/10.1002/adma.201901585.

DOI: 10.1002/adma.201901585

bilayer actuators suffers poor interlayer adhesion during frequent bending and unbending deformation, which sets a huge obstacle for their practical applications. Theoretically, the QSF effect has provided a hint that the adsorption and transmission of water molecules within a GO film can be tuned in a controlled fashion by building asymmetric QSF channels at nanoscale. In this case, new-type GO actuators can be produced without the use of other coupled materials or bilayer structures. However, to date, QSF enabled GO actuators have not been reported yet.

Here, we report moisture-responsive GO and MXene actuators based on QSF theory. To generate an asymmetric QSF channel network, we designed and fabricated unilaterally structured GO paper through a simple soft lithography method. By introducing folded nanostructures on one side of a GO paper, the adsorption, transmission, and desorption of water molecules, as well as its consequent deformation can be well controlled without coupling any other materials. In this way, moisture-responsive actuators enabling predictable deformation have been successfully developed based on GO and MXene.

Owing to the strong interaction between the oxygen groups on GO sheets and water molecules,[20] the diffuse rate of water molecules between GO sheets is reported to be ultrafast.[15] In this case, it is easy to understand that GO is quite sensitive to moisture. Previous works reported by our group and others have already proven that GO expands upon exposure to moisture. This phenomenon has been considered as the inherent mechanism for moisture-responsive actuators based on GO. However, to the best of our knowledge, the expansion mechanism of GO has not been clearly clarified yet. Unlike moisture-responsive hydrogels, GO film features a layered nanostructure because of the ordered stacking of GO sheets. Thus, the expansion of GO film along and against the normal direction of the film must follow distinct ways. To get further insight into the water adsorption induced swelling effect, we investigated the expansion manners both theoretically and experimentally. The possible water transmission path within a GO film that could be considered as the QSF channels for water molecules is shown in **Figure 1**a. Owing to the layered nanostructure, water molecules may mainly permeate through the defect region or the edge of neighboring GO sheets and diffuse between GO sheets interlayers. To explore the binding energy between a water molecule and different oxygen containing groups, we employed a first-principles study to quantify their binding energy (Figure 1b). Notably, the interaction between graphene (sp^2 region) and a water molecule is weak van der Waals force, ≈0.04 eV/H_2O. However, when a water molecule interacts with oxygen groups, much stronger hydrogen bond

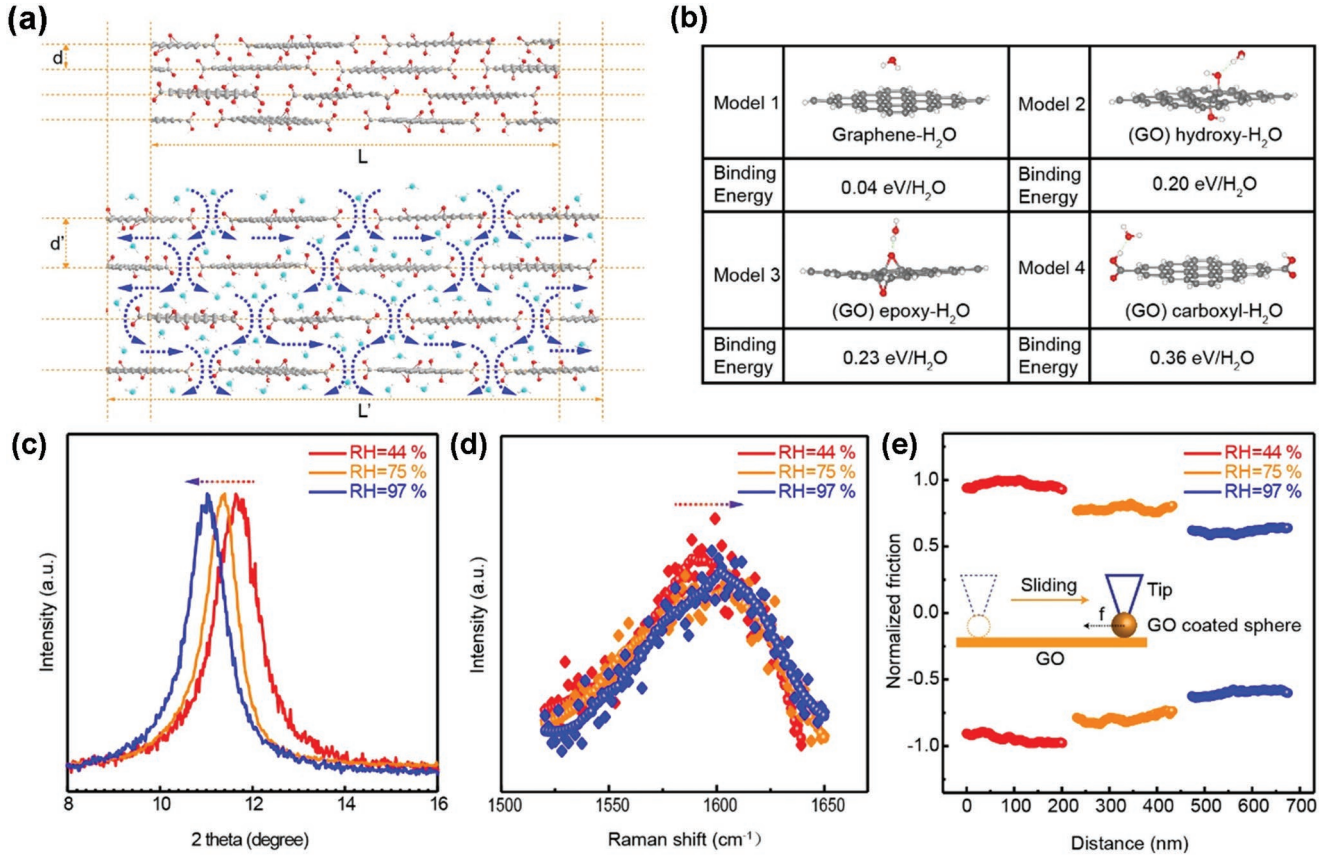

Figure 1. Quantum confined superfluidics in GO film. a) Schematic illustration of possible water transmission path (water QSF channel) within a GO film. b) First-principles study of the binding energy between a water molecule and graphene (sp^2 carbon) as well as GO with different oxygen groups. c) X-ray diffraction patterns and d) Raman spectra of GO film under different humidity, RH = 44%, 75%, and 97%, respectively. e) Lateral friction force of forward and backward scanning a GO coated silica sphere tip on GO film under different humidity, RH = 44%, 75%, and 97%, respectively.

would form. The binding energies of hydroxyl, epoxy, and carboxyl groups on a GO nanosheets with H_2O molecule are 0.20 eV/H_2O, 0.23 eV/H_2O, and 0.36 eV/H_2O, respectively, among which the binding energy between carboxyl and water molecule is the highest, about 9 times of that with sp^2 carbon. In this regard, we can reasonably deduce that water molecules show much stronger interaction with the edge of GO sheets where the carboxyl groups mainly appears.

To get deep insight into the expansion of GO under moisture actuation, we collected the X-ray diffraction (XRD) patterns of a GO film under different humidity conditions (RH = 44%, 75%, and 97%, Figure 1c and Figure S1a, Supporting Information). The interlayer spacing of GO nanosheets increase from 7.56 to 8.03 Å when the RH increased from 44% to 97% due to the adsorption of water molecules.[24,29] According to classical hydrodynamics, the transport of water molecules across such a narrow interlayer space should be very slow.[33] Nevertheless, according to Geim and coworkers results,[15] the GO membranes allowed ultrafast water permeation. The ultrafast flow of water in the confined interlayer space can be considered as "quantum tunneling fluidics effect."[34] The adsorption and ultrafast transport of water molecules further increased the interlayer spacing. However, considering the layered structure of GO, the increase of d-spacing would only increase the film thickness (expansion along the normal direction), which cannot lead to the mismatch of strain at the bilayer interface. Therefore, the bending of the GO bilayer actuators (e.g., GO and RGO bilayer) should originate from the inner stress of GO sheets or the sliding between neighboring GO nanosheets. To confirm this hypothesis, we further characterized the GO film by Raman spectra under different relative humidity conditions (Figure 1d, and Figure S1b, Supporting Information). According to the reported results, the shift of G peak can be attributed to doping, temperature change and strain.[35–38] In this work, when the surrounding humidity increased, the G peak slightly shifts from 1600.7 cm^{-1} (RH = 44%) to 1602.72 cm^{-1} (RH = 97%). Considering the strong interaction between the edges of GO sheets and water molecules, the blueshift of the G peak suggests that inner stress release under high humidity. Besides, to quantify the interlayer resistance that hinder the sliding of GO sheets, we also measured the friction force between overlap GO nanosheets under different humidity using atomic force microscopy (AFM). As shown in Figure 1e, the AFM tip was equipped with a SiO_2 sphere (≈30 µm in diameter) and coated with GO. Then, the GO coated sphere tip was used to slide on GO nanosheets to measure the interlayer sliding resistance. Notably, with the increase of RH from 44% to 97%, the lateral force between GO nanosheets decreased ≈40%. This result is in good agreement with our hypothesis. The presence of lubricating water layer can result in the increase of d-spacing and significantly decrease the interlayer friction, which can facilitate the sliding of GO sheets. In this case, the expansion of GO films under moisture actuation becomes clear. Along the normal direction, GO may become thick after water adsorption due to the increase of d-spacing. While along the GO sheets plane, adsorption of water molecule can lead to tangential stress due to the inner stress and the sliding of GO nanosheets. The stress along the tangential direction accounts for the bending performance. To confirm this hypothesis, controlled experiments have been carried out. We prepared Fe^{3+} linked GO and pure GO bilayer actuators. The cross-linking of GO sheets by Fe^{3+} would significantly prevent the interlayer sliding effect due to the strong electrostatic attraction, moisture induced sliding of GO nanosheets can be suppressed, and thus the bilayer should bend toward the linked side. The experimental result is the same (Figure S1c–e, Supporting Information). The deep understanding of the GO swelling mechanism inspired us to tailor the stress along the tangential direction by engineering the QSF channels within a GO film, providing the possibility for developing moisture-responsive actuators only using GO.

As discussed above, the moisture induced deformation of GO mainly depends on the stress mismatch along the tangential direction of GO sheets. Therefore, to realize predictable deformation of GO, the QSF channels that govern the adsorption and transmission of water molecules should be tailored controllably within GO films. As shown in **Figure 2**, a unilaterally structured GO film was prepared by soft lithography using poly(dimethylsiloxane) (PDMS) gratings with variable periods as templates (Figure S2a, Supporting Information). First, GO aqueous solutions was cast on the PDMS template and dried in air, forming an asymmetrically structured GO film. Then, the unilaterally structured GO film was peeled off from the PDMS template (Figure 2a). The entire fabrication process is simple and free of chemicals. Therefore, the chemical composition of the unilaterally structured GO film keeps unchanged with that of pristine GO. The properties of both flat and structured GO have been characterized by the Fourier transform infrared (FTIR) spectroscopy and X-ray photoelectron spectroscopy (XPS) results (Figures S3 and S4, Supporting Information). Figure 2b–d shows the confocal laser scanning microscopy (CLSM) images of the structured GO films. Microgratings with periods of 20, 40, and 100 µm can be observed clearly. The profile of these gratings is 3, 5, and 9 µm in height, respectively. Scanning electron microscopy (SEM) images of the structured side further confirm the presence of the gratings. On the contrary, the back side of film is almost flat (Figure S5, Supporting Information). Here, we used the area ratios between the structured side and the flat side to evaluate the roughness of these GO films. According to the profiles of these three samples (20, 40, and 100 µm period), the area ratios are 1.08, 1.13, and 1.03, respectively (Figure 2e–j). The ordered grating structures cause additional wrinkles, which can act as QSF channels and facilitate the adsorption and transportation of water. In this way, the asymmetrical GO film bends to the flat side when RH increases. Notably, the unilaterally structured GO film (12 × 1 mm) with a period of 40 µm demonstrated the largest curvature, ≈8.7 cm^{-1}, at high humidity, RH = 97%, since it has the highest area ratio of 1.13 (Figure 2k). The response is reversible and the response time is quite short, it takes only 7 s to reach the maximum curvature, and can recover to the flat state within 4 s by switching the relative humidity between RH = 23% and RH = 97% (Figure 2l). The fast response can be attributed to the ultrafast transport of water molecules across the ultranarrow interlayer space of GO (7.56–8.03 Å), which is considered as "quantum tunneling fluidics effect." To quantify the water adsorption capacity of these structured GO films, we measured the water adsorption–desorption isotherms of the samples (Figure 2m). All the structured GO show higher

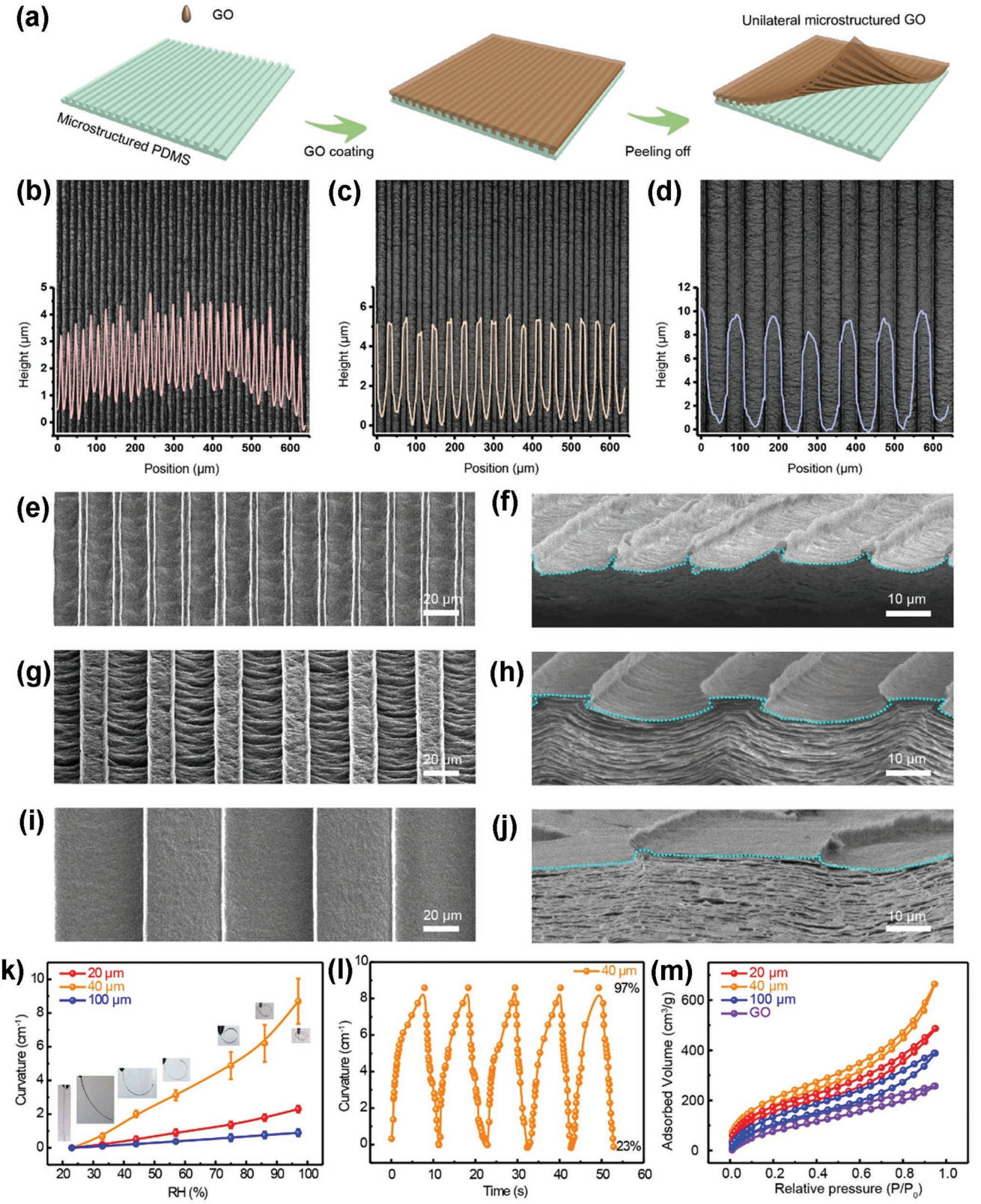

Figure 2. Fabrication, characterization, and moisture-responsive actuation of asymmetrical structured GO film. a) Schematic illustration of the fabrication of structured GO film. b–d) The confocal laser scanning microscopy (CLSM) images of structured GO film with periods of 20 μm (b), 40 μm (c), and 100 μm (d). e–j) Top and section view SEM images of structured GO film with periods of 20 μm (e,f), 40 μm (g,h), and 100 μm (i,j). k) Dependence of the curvature on RH. The insets are photographs of curved ribbons under different humidity. l) Plot of curvature against time for the structured GO film (T = 40 μm). RH was switched between 23% and 97%. m) Water adsorption–desorption isotherms of the structured and flat GO films.

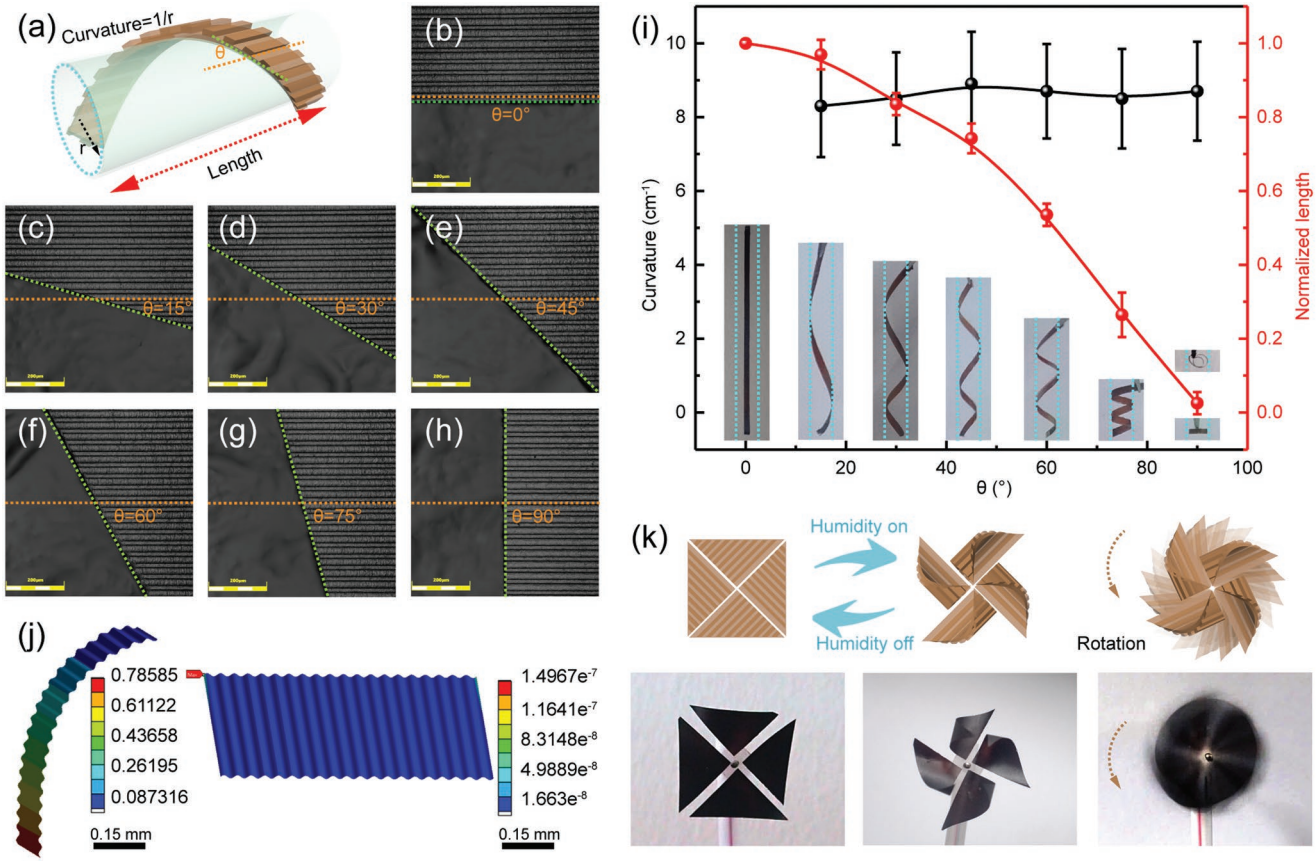

Figure 3. Controllable shape deformation of the unilaterally structured GO paper. a) Schematic illustration of the twisting of a unilaterally structured GO ribbon in response to the moisture. b–h) CLSM images of the edge of the structured GO film with different cross angles (θ). i) Dependence of curvature and normalized length on the cross angles (θ) under moisture actuation. The insets are relative photographs. j) FEA results of the shape deformation associated with the bending of the structured GO film. k) Schematic illustration of the assembly and response of humidity-responsive windmills, as well as the real photographs of this smart windmills in dry air, under moisture actuation and under moisture blowing.

adsorption of water than the flat GO, in which the structured GO film with a period of 40 µm shows the highest water adsorption capacity, in good agreement with their response property under high moisture (Figure S6, Supporting Information).

The moisture-responsive deformation of the unilaterally structured GO paper can be controlled by the orientation of the GO gratings (**Figure 3**a). We prepared the structured GO film with different orientations, in which the cross angle between grating and the edge (θ) varies from 0° to 90° (Figure 3b–h). Under moisture actuation, the ribbons twisted to different states (Figure 3i). Interestingly, the curvature viewed along the axis keeps a constant value, whereas the normalized length along the axis decreased with the cross angle θ. We explain the mechanism for the orientation-defined shape deformation by finite element analysis (Figure 3j). Along the direction parallel to the structure, the film can deform 0.786 mm under $3.2e^{-15}$ N loading force, whereas, along the perpendicular direction, only 0.15 nm deformation can be achieved under the same condition. Owing to the mechanical confinement, the unilaterally structured GO paper may prefer to bend against the grating direction upon moisture actuation. Taking advantage of this orientation-defined deformation, we prepared four triangular films with different grating orientation and assembled them together (Figure 3k). Interestingly, it deforms into a windmill under high humidity and rotates when blowing moisture.

To demonstrate its full potential in developing soft robots, we designed and prepared two kinds of smart GO ribbons with chiral twisting behaviors as legs for assembling a centipede mini-robot. As shown in **Figure 4**a, ten pairs of chiral twisting ribbons were attached on a paper body to form a centipede. We control this moisture-responsive centipede using a self-made moisture supplying system (Figure S7, Supporting Information). For the actuation of this centipede, the flow speeds for breathing in and out are 0.4 and 0.2 m s^{-1}, respectively. Under moisture actuation, the smart centipede can crawl toward the right side (Figure 4b and Video S1, Supporting Information). Unlike some other actuators that can move due to frequent bending and unbending deformation, the centipede mini-robot can crawl forward due to the cooperation of the chiral twisting legs, because the interaction between their legs and the substrate during humidifying and drying cycles is asymmetric (Figure S8, Supporting Information). We further investigate the crawling track by marking a red point at the back-antennae. As shown in Figure 4c, the centipede moves uniformly, the speed is calculated to be 0.98 mm s^{-1}. Additionally, the twisting of the left and right legs is rhythmic. Figure S7 (Supporting

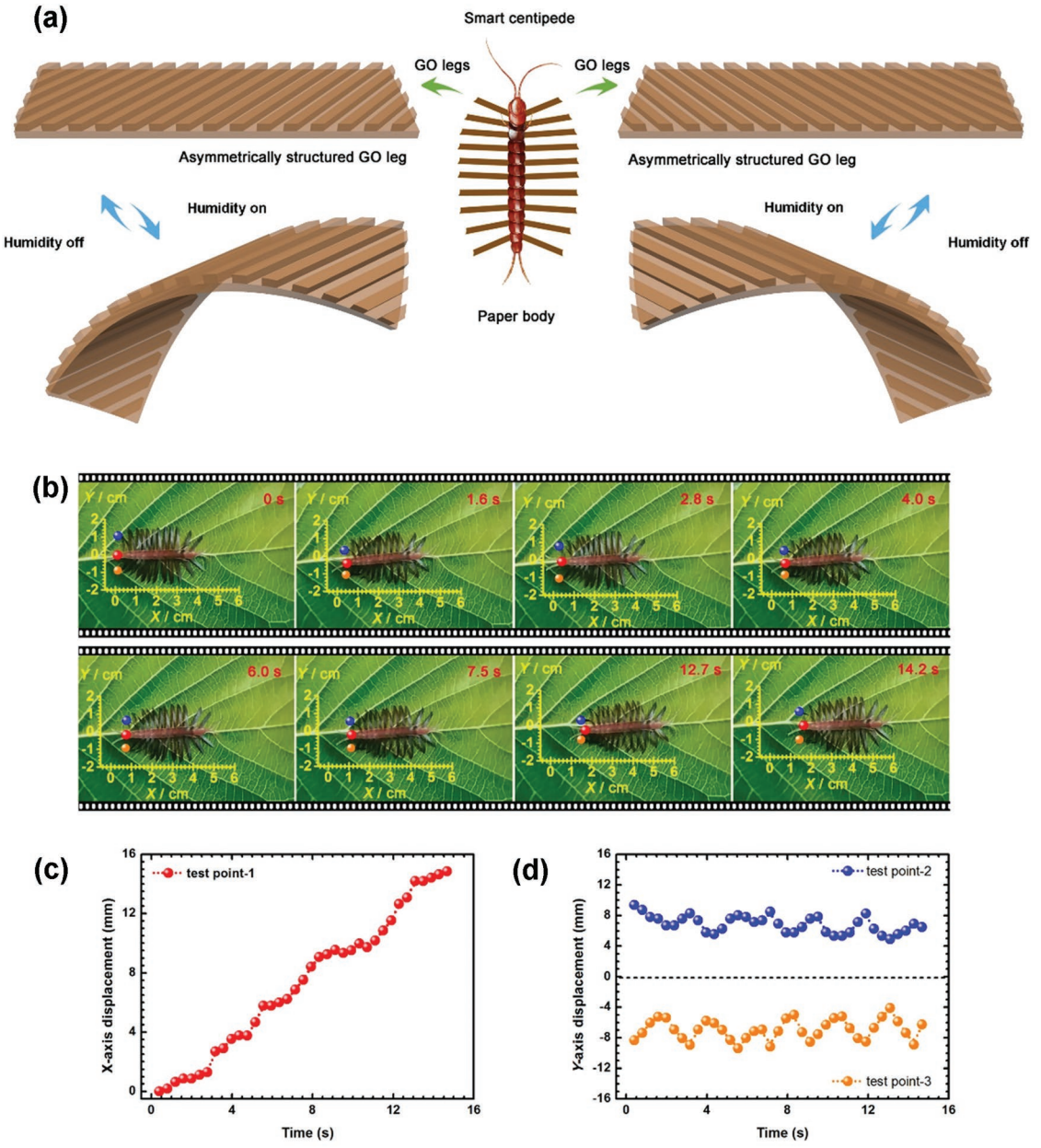

Figure 4. A centipede-like soft mini-robot based on the smart GO paper. a) Schematic illustration of moisture-responsive smart legs of the centipede mini-robot. b) Snapshots of the crawling centipede mini-robot with smart GO legs. c) Displacement change of the back-antennae (red point) along the *X* axis with time. d) Displacement change of the backfoot (blue and orange points) along the *Y* axis with time.

Information) shows the scheme for the local moisture control. By breathing in and out moisture through a "Y"-shape channel, we can control the humidity around the worm. We marked the last two pairs of legs by a blue and an orange point, respectively, as shown in Figure 4d. The rhythmic switching of humidity (Figure S9, Supporting Information) can trigger periodic twisting of the legs, leading to steadily walking along a straight line at a uniform speed.

Drosera, usually known as the sundews can deform their tentacles under the stimulation of prey. Their tentacles can bend to catch small insects.[39,40] Inspired by *Drosera,* we prepared a GO smart leaf that permits moisture actuation and enables catching live insect (**Figure 5**a and Video S2, Supporting Information). Creating grating structure is not the only choice for tailoring the QSF channel of GO paper. Unilaterally structured smart GO paper can be prepared through a more facile way. Here, a general metal wire mesh (Figure S10, Supporting Information) is also workable for templating the asymmetrical structures on a GO paper. Figure 5b demonstrates a large-area smart GO paper prepared through this way, the diameter is ≈14.5 cm. The as-obtained GO paper is quite sensitive to moisture (Figure S11, Supporting Information), it bends rapidly when it was close to a palm (Figure 5c,d). After exposure to high humidity (RH = 97%), it can reach a maximum curvature of ≈8.6 cm^{-1} within

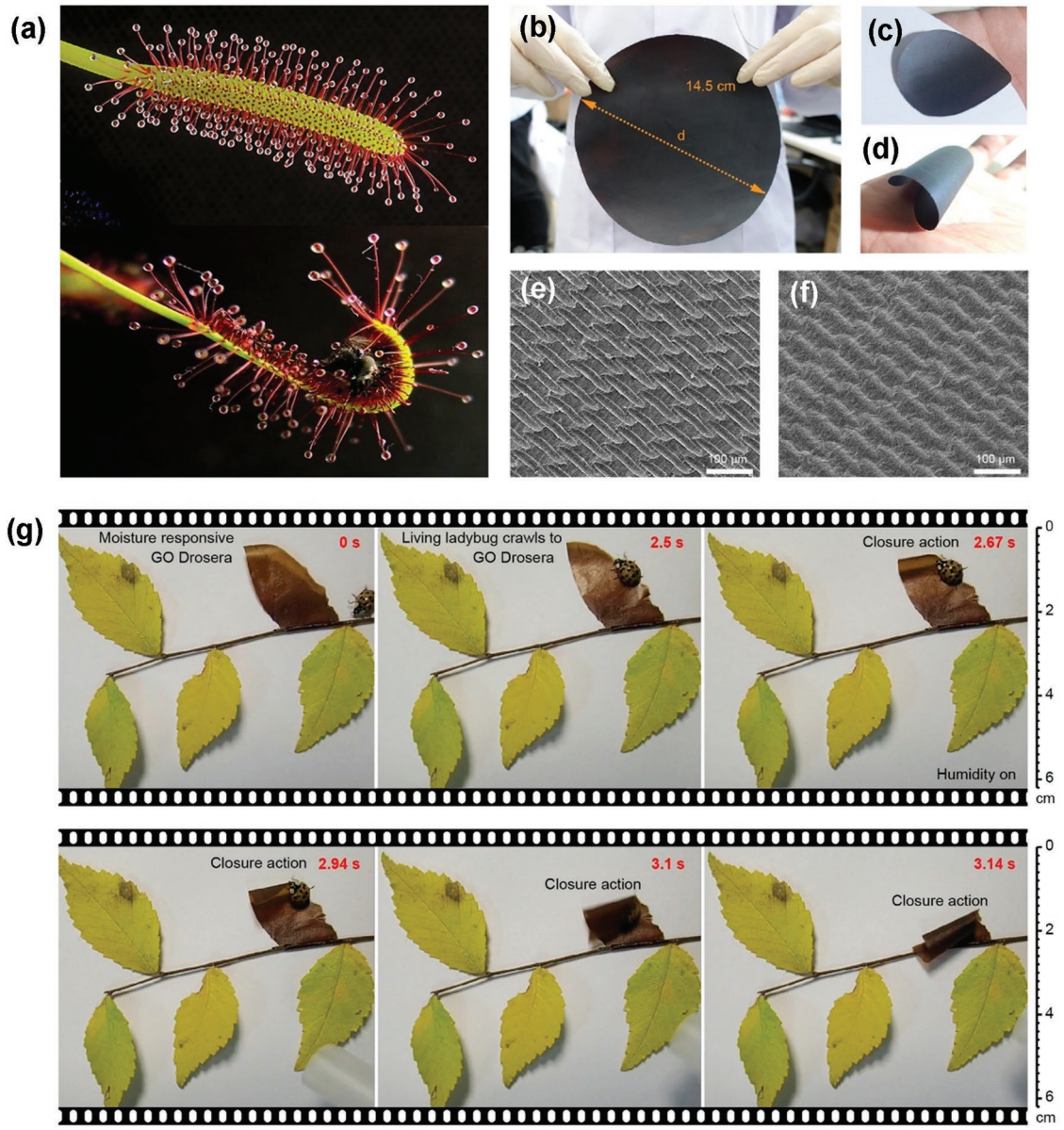

Figure 5. Large-area preparation of the smart GO paper and a demonstration of smart leaf. a) Photographs of *Drosera* that can deform under stimuli. b) Large-area smart GO paper. c,d) The deformation of the smart GO paper on a dry paper (c) and on the palm (d). e,f) SEM image of the smart GO paper prepared using mesh as a template: e) the upper side, and f) the back. g) A smart GO leaf shape that can catch the living ladybug.

7 s. Compared to shape memory alloy film,[41] the actuator based on structured GO shows longer response time, but much higher bending curvature at room temperature. SEM images confirm the asymmetrical structures on both sides of the GO paper (Figure 5e,f). Similar with the smart GO paper with grating structures, the GO paper templated by wire mesh also demonstrates orientation-defined deforming property, which provides the feasibility for design biomimetic smart devices. In addition to the asymmetrical structures, both the size and the oxygen content of GO can influence the moisture-responsive properties. The GO used in this work (Figure S12, Supporting Information) is prepared from fine graphite powder (<10 μm). For control experiments, we also prepared GO sheets with less oxygen (Figure S13, Supporting Information) and large GO sheets (Figure S14, Supporting Information). According to our experimental results, GO with more OCGs and smaller size is of benefit to the moisture response properties (Figure S15, Supporting Information).

Figure 5g shows the video snapshots genius of the moisture response of the smart GO leaf. The detailed scheme for the moisture supplying system for this smart leaf is shown in the Figure S16 (Supporting Information). The flow speed of humid air used to smart leaf is about 0.7 m s^{-1}. Owning to the ultrafast bending velocity and the large deforming degree, the smart leaf bent rapidly under the moisture actuation. It can trap a living ladybug when it passed by the smart GO leaf. The whole catching process occurs within 0.5 s, indicating its fast response. After the living ladybug crawled over the smart

leaf, no detectable traces can be observed on the GO surface (Figure S17, Supporting Information); and the GO smart leaf is workable after repeated catching and releasing performance. Here, the weight of a living ladybug is about 0.025 g; and the contact area for each foot is about 100 × 350 µm. Thus, the pressure is estimated to be ≈1200 Pa (six legs). Considering the fact that GO owns high effective Young's modulus (207.6–23.4 GPa),[42,43] the local contact of the bug with the GO has no specific influence.

The method reported in this paper is universal. We further demonstrated the fabrication of unilaterally structured MXene paper and investigated their moisture-responsive properties. Similar with GO, MXene is another type of 2D materials that shows strong interaction with water molecules. Take $Ti_3C_2T_x$ (T_x, e.g., –O,–OH, and –F) as an example, the adsorption and transportation of water molecules in the QSF channel between layered $Ti_3C_2T_x$ nanosheets would lead to obvious layer expansion (Figure S18a, Supporting Information). To confirm this assumption, we measured the d-spacing of $Ti_3C_2T_x$ paper in different RHs (Figure S18b, Supporting Information). The d-spacing of $Ti_3C_2T_x$ paper is about 11.98 nm (RH = 44%), whereas the d-spacing of $Ti_3C_2T_x$ paper is about 12.21 nm under RH = 97%. We fabricated the unilaterally structured $Ti_3C_2T_x$ paper through the same method using wire mesh as a template (Figure S18c,d, Supporting Information). The unilaterally structured $Ti_3C_2T_x$ paper demonstrates fast and reversible moisture-responsive ability (Figure S18e,f, Supporting Information). Essentially, the moisture response properties of MXene also relay on the strong interaction between water molecules and the oxygen groups on MXene sheets. Here, the unilaterally structured $Ti_3C_2T_x$ paper demonstrated the maximum curvature of ≈2.1 cm^{-1} at high humidity (RH = 97%), which is about a quarter of that of GO (Figure S18e, Supporting Information). It takes about 12 s to reach the maximum curvature, and recovers to the flat state within 11 s upon switching the relative humidity between RH = 23% and RH = 97%. As compared with GO, MXene-based actuators shows smaller deformation and longer response time. The performance differences can be attributed to differences in the contents of oxygen groups and the interlayer d-spacing. According to the published results,[44–46] MXene possesses less oxygen groups and larger interlayer d-spacing.

In summary, based on the theoretical and experimental investigation on the GO expansion mechanism upon water adsorption, a simple soft lithography method has been employed for asymmetrically tailoring the QSF channels of GO films toward controlling the selective water adsorption and transmission. The resultant unilaterally structured GO films demonstrated sensitive moisture-responsive properties. State-of-the-art of ultrafast bending velocity (Table S1, Supporting Information) and orientation-defined and predictable deformation has been achieved, revealing the potential for developing smart soft robots. As a proof of concept, a moisture-responsive centipede robot with chiral bending GO legs and a smart leaf capable of catching a living ladybug have been successfully fabricated. Additionally, the unilaterally structuring method for QSF channel tailoring permits scaling up, a 14.5 cm smart GO film can be readily prepared using structured templates such as metal wire mesh. Overall, we deem that flexible tailoring the QSF channels of GO holds great promise for developing GO-based smart devices and systems beyond actuators, energy storage and water desalination.

Experimental Section

Fabrication of PDMS Templates: The PDMS templates were fabricated via a soft lithography method using PDMS elastomer (Sylgard 184 Silicone Elastomer, Dow Corning Corporation). The PDMS prepolymer was mixed with a curing agent (10:1 by weight), which was poured at the surface of silicon templates and cured at 80 °C for 40 min. The structured PDMS templates were peeled off from the silicon templates for further usage.

Preparation of GO: GO was prepared via the Hummers method. Two kinds of graphite (≈10 and ≈100 µm) were used as raw materials. 2 g of graphite powder, 2 g of $NaNO_3$, and 96 mL of concentrated H_2SO_4 (98%) were mixed at ≈0 °C. Then, 12 g of $KMnO_4$ was slowly added into the mixture at 0 °C for 90 min, and kept at 35 °C for additional 120 min. After that, 80 mL of distilled water was slowly added into the mixture. 10 mL of H_2O_2 (30%) was slowly dropped into the mixture. Finally, GO aqueous solution was obtained by repeatedly washed with distilled water and high-speed centrifugation until the pH reaches 7.

Preparation of GO Membranes: GO aqueous solution was poured at the surface of structured PDMS and dried by air. The structured GO membranes were peeled before using.

Preparation of MXene Membranes: The $Ti_3C_2T_x$ aqueous solution was purchased from 11 Technology Co., Ltd (Jilin, China). The structured MXene ($Ti_3C_2T_x$) paper was prepared by pour $Ti_3C_2T_x$ aqueous solution at the surface of structured mesh with a mesh size of 2800 mesh and dried by air. The structured $Ti_3C_2T_x$ membranes were peeled before using.

Characterization: Powder XRD patterns were obtained from a Rigaku D/MAX 2550 diffractometer with Cu Kα radiation (λ = 1.5418 Å). Raman was measured by LabRAM HR Evolution. Confocal laser scanning microscopy images were investigated by Olympus OLS4100 LEXT 3D measuring laser microscope. SEM images obtained from the JEOL JSM7500 field-emission scanning electron microscope. IR spectroscopy was measured using a Nicolet iS50 FT-IR spectrometer. XPS was performed by an ESCALAB 250 spectrometer. The relative humidity environments were made by the saturated aqueous solutions, for example, CH_3COOK (RH = 23%), $MgCl_2$ (RH = 33%), K_2CO_3 (RH = 44%), NaBr (RH = 57%), NaCl (RH = 75%), KCl (RH = 86%), and K_2SO_4 (RH = 97%), respectively. The moisture-responsive GO film was cut into ribbons (12 × 1 mm) for bending tests. All the measurements were conducted in air at room temperature (25 °C).

Supporting Information

Supporting Information is available from the Wiley Online Library or from the author.

Acknowledgements

The authors thank Zhan-Dong Li and Yu Song for the characterization of the lateral force between GO nanosheets under different RH. The authors acknowledge the National Key Research and Development Program of China and National Natural Science Foundation of China under Grants #2017YFB1104300, #61775078, #61590930, #61605055, and #61435005 for support. The experiments involving live ladybugs were approved by the Institutional Animal Care and Use Committee of Jilin University (Number of permit, 20160930).

Conflict of Interest

The authors declare no conflict of interest.

Keywords

creeping centipede, moisture actuation, quantum confined superfluidics, smart leaves, structured graphene oxide paper

Received: March 12, 2019
Revised: May 7, 2019
Published online: June 13, 2019

[1] K. Venkatachalam, C. Montell, *Annu. Rev. Biochem.* **2007**, *76*, 387.
[2] R. Henderson, *Nature* **2013**, *504*, 93.
[3] T. B. H. Schroeder, A. Guha, A. Lamoureux, G. VanRenterghem, D. Sept, M. Shtein, J. Yang, M. Mayer, *Nature* **2017**, *552*, 214.
[4] J. Xu, D. A. Lavan, *Nat. Nanotechnol.* **2008**, *3*, 666.
[5] A. L. Gotter, M. A. Kaetzel, J. R. Dedman, *Comp. Biochem. Physiol., Part A: Mol. Integr. Physiol.* **1998**, *119*, 225.
[6] A. G. Volkov, J. C. Foster, T. A. Ashby, R. K. Walker, J. A. Johnson, V. S. Markin, *Plant, Cell Environ.* **2010**, *33*, 163.
[7] W. S. Y. Wong, M. F. Li, D. R. Nisbet, V. S. J. Craig, Z. K. Wang, A. Tricoli, *Sci. Adv.* **2016**, *2*, e1600417.
[8] Y. Temmei, S. Uchida, D. Hoshino, N. Kanzawa, M. Kuwahara, S. Sasaki, T. Tsuchiya, *FEBS Lett.* **2005**, *579*, 4417.
[9] X. Zhang, H. Liu, L. Jiang, *Adv. Mater.* **2019**, *31*, 1804508.
[10] K. Xiao, G. H. Xie, Z. Zhang, X. Y. Kong, Q. Liu, P. Li, L. P. Wen, L. Jiang, *Adv. Mater.* **2016**, *28*, 3345.
[11] Y. F. Wu, D. Y. Wang, I. Willner, Y. Tian, L. Jiang, *Angew. Chem., Int. Ed.* **2018**, *57*, 7790.
[12] G. H. Xie, P. Li, Z. J. Zhao, Z. P. Zhu, X. Y. Kong, Z. Zhang, K. Xiao, L. P. Wen, L. Jiang, *J. Am. Chem. Soc.* **2018**, *140*, 4552.
[13] K. Celebi, J. Buchheim, R. M. Wyss, A. Droudian, P. Gasser, I. Shorubalko, J. I. Kye, C. Lee, H. G. Park, *Science* **2014**, *344*, 289.
[14] S. P. Surwade, S. N. Smirnov, I. V. Vlassiouk, R. R. Unocic, G. M. Veith, S. Dai, S. M. Mahurin, *Nat. Nanotechnol.* **2015**, *10*, 459.
[15] R. R. Nair, H. A. Wu, P. N. Jayaram, I. V. Grigorieva, A. K. Geim, *Science* **2012**, *335*, 442.
[16] J. Abraham, K. S. Vasu, C. D. Williams, K. Gopinadhan, Y. Su, C. T. Cherian, J. Dix, E. Prestat, S. J. Haigh, I. V. Grigorieva, P. Carbone, A. K. Geim, R. R. Nair, *Nat. Nanotechnol.* **2017**, *12*, 546.
[17] Q. Yang, Y. Su, C. Chi, C. T. Cherian, K. Huang, V. G. Kravets, F. C. Wang, J. C. Zhang, A. Pratt, A. N. Grigorenko, F. Guinea, A. K. Geim, R. R. Nair, *Nat. Mater.* **2017**, *16*, 1198.
[18] J. Feng, M. Graf, K. Liu, D. Ovchinnikov, D. Dumcenco, M. Heiranian, V. Nandigana, N. R. Aluru, A. Kis, A. Radenovic, *Nature* **2016**, *536*, 197.
[19] W. S. Hummers, R. E. Offeman, *J. Am. Chem. Soc.* **1958**, *80*, 1339.
[20] L. Guo, H. B. Jiang, R. Q. Shao, Y. L. Zhang, S. Y. Xie, J. N. Wang, X. B. Li, F. Jiang, Q. D. Chen, T. Zhang, H. B. Sun, *Carbon* **2012**, *50*, 1667.
[21] H. B. Huang, Z. G. Song, N. Wei, L. Shi, Y. Y. Mao, Y. L. Ying, L. W. Sun, Z. P. Xu, X. S. Peng, *Nat. Commun.* **2013**, *4*, 9.
[22] A. Lerf, A. Buchsteiner, J. Pieper, S. Schottl, I. Dekany, T. Szabo, H. P. Boehm, *J. Phys. Chem. Solids* **2006**, *67*, 1106.
[23] A. Buchsteiner, A. Lerf, J. Pieper, *J. Phys. Chem. B* **2006**, *110*, 22328.
[24] J. Deng, Y. You, H. Bustamante, V. Sahajwalla, R. K. Joshi, *Chem. Sci.* **2017**, *8*, 1701.
[25] L. Qu, Y. Liang, F. Zhao, Z. Cheng, Y. Deng, Y. Xiao, H. Cheng, P. Zhang, Y. Huang, H. B. Shao, *Energy Environ. Sci.* **2018**, *11*, 1730.
[26] W. Gao, N. Singh, L. Song, Z. Liu, A. L. M. Reddy, L. J. Ci, R. Vajtai, Q. Zhang, B. Q. Wei, P. M. Ajayan, *Nat. Nanotechnol.* **2011**, *6*, 496.
[27] L. Wang, X. P. Lu, C. J. Wen, Y. Z. Xie, L. F. Miao, S. H. Chen, H. B. Li, P. Li, Y. H. Song, *J. Mater. Chem. A* **2015**, *3*, 608.
[28] D. D. Han, Y. L. Zhang, J. N. Ma, Y. Liu, J. W. Mao, C. H. Han, K. Jiang, H. R. Zhao, T. Zhang, H. L. Xu, H. B. Sun, *Adv. Mater. Technol.* **2017**, *2*, 1700045.
[29] B. Mi, *Science* **2014**, *343*, 740.
[30] H. H. Cheng, J. Liu, Y. Zhao, C. G. Hu, Z. P. Zhang, N. Chen, L. Jiang, L. T. Qu, *Angew. Chem., Int. Ed.* **2013**, *52*, 10482.
[31] D. D. Han, Y. L. Zhang, Y. Liu, Y. Q. Liu, H. B. Jiang, B. Han, X. Y. Fu, H. Ding, H. L. Xu, H. B. Sun, *Adv. Funct. Mater.* **2015**, *25*, 4548.
[32] D. D. Han, Y. L. Zhang, H. B. Jiang, H. Xia, J. Feng, Q. D. Chen, H. L. Xu, H. B. Sun, *Adv. Mater.* **2015**, *27*, 332.
[33] M. Majumder, N. Chopra, R. Andrews, B. J. Hinds, *Nature* **2005**, *438*, 44.
[34] L. P. Wen, X. Q. Zhang, Y. Tian, L. Jiang, *Sci. China Mater.* **2018**, *61*, 1027.
[35] M. Goldsche, J. Sonntag, T. Khodkov, G. Verbiest, S. Reichardt, C. Neumann, T. Ouaj, N. D. D. Von, D. Buca, C. Stampfer, *Nano Lett.* **2018**, *18*, 1707.
[36] D. Fei, H. Ji, Y. Chen, A. Herklotz, K. Dörr, Y. Mei, A. Rastelli, O. G. Schmidt, *Nano Lett.* **2010**, *10*, 3453.
[37] H. Komurasaki, T. Tsukamoto, K. Yamazaki, T. Ogino, *J. Phys. Chem. C* **2012**, *116*, 10084.
[38] Y. Gao, L. Q. Liu, S. Z. Zu, K. Peng, D. Zhou, B. H. Han, Z. Zhang, *ACS Nano* **2011**, *5*, 2134.
[39] Y. Nakamura, M. Reichelt, V. E. Mayer, A. Mithofer, *Proc. R. Soc. B* **2013**, *280*, 20130228.
[40] M. Krausko, Z. Perutka, M. Sebela, O. Samajova, J. Samaj, O. Novak, A. Pavlovic, *New Phytol.* **2017**, *213*, 1818.
[41] H. Takagi, K. Okano, S. Juodkazis, S. Matsuo, H. Misawa, *Adv. Eng. Mater.* **2003**, *5*, 732.
[42] J. W. Suk, R. D. Piner, J. H. An, R. S. Ruoff, *ACS Nano* **2010**, *4*, 6557.
[43] N. V. Medhekar, A. Ramasubramaniam, R. S. Ruoff, V. B. Shenoy, *ACS Nano* **2010**, *4*, 2300.
[44] F. Shahzad, M. Alhabeb, C. B. Hatter, B. Anasori, S. M. Hong, C. M. Koo, Y. Gogotsi, *Science* **2016**, *353*, 1137.
[45] M. Alhabeb, K. Maleski, B. Anasori, P. Lelyukh, L. Clark, S. Sin, Y. Gogotsi, *Chem. Mater.* **2017**, *29*, 7633.
[46] M. Ghidiu, S. Kota, V. Drozd, M. W. Barsoum, *Sci. Adv.* **2018**, *4*, eaao6850.